

Controlled support of a magnetic fluid at a superhydrophobic interface

Cite as: Appl. Phys. Lett. **116**, 221601 (2020); <https://doi.org/10.1063/5.0005639>

Submitted: 23 February 2020 . Accepted: 24 May 2020 . Published Online: 02 June 2020

Qingwen Dai , Zhengdong Hu, Wei Huang, and Xiaolei Wang 



View Online



Export Citation



CrossMark

Lock-in Amplifiers
up to 600 MHz



Controlled support of a magnetic fluid at a superhydrophobic interface

Cite as: Appl. Phys. Lett. **116**, 221601 (2020); doi: [10.1063/5.0005639](https://doi.org/10.1063/5.0005639)

Submitted: 23 February 2020 · Accepted: 24 May 2020 ·

Published Online: 2 June 2020



View Online



Export Citation



CrossMark

Qingwen Dai,  Zhengdong Hu, Wei Huang,^{a)} and Xiaolei Wang 

AFFILIATIONS

National Key Laboratory of Science and Technology on Helicopter Transmission, Nanjing University of Aeronautics and Astronautics, Nanjing 210016, China

^{a)} Author to whom correspondence should be addressed: huangwei@nuaa.edu.cn

ABSTRACT

In this paper, the controlled support of a magnetic fluid at a superhydrophobic interface is proposed. It is shown experimentally that the support of the magnetic fluid has excellent dynamic response characteristics and can be enhanced by increasing the magnetic field intensity. Numerical simulations are performed to clarify how the magnetic field is distributed, and the support mechanism is revealed theoretically. This study provides further physical insight into liquid-based support and offers excellent prospects for frictionless and controllable micro-platforms and laboratory-on-chip applications.

Published under license by AIP Publishing. <https://doi.org/10.1063/5.0005639>

Manipulating tiny amounts of liquids is becoming a topic of intense research interest because unique functions can be realized in a compact space.^{1–5} The interaction between a liquid and a solid is always accompanied by interfacial adhesion, on the basis of which many applications are realized, including surface adhesion,⁶ self-assembly,⁷ and mechanical strengthening.⁸ In other cases, one may wish to eliminate the adhesion intentionally and replace it with a supporting capacity.⁹ For instance, in micro-bearings, creating a liquid support between the rubbing surfaces would improve the tribological performance.¹⁰

The adhesion and supporting forces originate mainly from the surface tension of liquids. Placing a liquid at a hydrophilic or hydrophobic interface gives rise to an adhesive or supporting force, respectively. In particular, the supporting capacity is highly dependent on the hydrophobic property, and one of the most direct and efficient ways to maximize the supporting force is to construct a superhydrophobic interface.¹¹ However, common liquids are unstable at a superhydrophobic interface: with even a slight inclination or compression, they either slide off or are squeezed off. Therefore, a precursor to achieving stable support is to be able to confine the liquid to the interface.

A magnetic fluid is a colloidal suspension of magnetic particles (mean diameter: ~ 10 nm) dispersed in a carrier liquid.^{12–14} Under an appropriate external magnetic field, it can be positioned in and limited to designated regions.^{15–17} By combining the advantages of an external magnetic field and a superhydrophobic interface, a magnetic fluid might be a feasible means of providing controllable support.

Herein, we design a magnetic fluid-based support at a superhydrophobic interface. As shown in Fig. 1(a), the substrates are made of polytetrafluoroethylene (PTFE) with dimensions of $15\text{ mm} \times 15\text{ mm} \times 1\text{ mm}$. Because of its relatively low friction coefficient (0.01) and high corrosion resistance, PTFE is used widely in many engineering applications, such as piston rings, clutches, micro-bearings, and guide ways.¹⁸ The upper PTFE is fixed on a glass plate and mounted at the end of a double parallel cantilever with a small mirror. The lower one is fixed on the top of a polymethyl methacrylate (PMMA) chamber inside which magnets are confined. The chamber is placed on a mobile platform. Cylindrical magnets (N35 NdFeB; axial magnetization; diameter: 4 mm; thickness: 1 mm) are used for the tests, and the magnetic field intensity is controlled by varying the number N of magnets ($N = 1, 2, 6, \text{ or } 10$). Based on the theory of magnetic charge, for a cylindrical magnet, the demagnetizing factors decrease with increasing axial thickness of the magnet.

The initial PTFE surfaces are smooth with an average surface roughness of $\sim 0.8\ \mu\text{m}$. The superhydrophobic surfaces are fabricated using ultraviolet laser machining [Fig. 1(b-①)] with an output power of 3 W, a frequency of 40 kHz, a pulse width of $0.5\ \mu\text{s}$, and a processing speed of 1000 mm/s. After laser processing, rough PTFE surfaces with an average surface roughness of $\sim 2.8\ \mu\text{m}$ are achieved. Figure 1(b-②) shows the wetting property and progressively enlarged scanning electron microscopy images of the prepared PTFE surface (the result of energy-dispersive x-ray spectroscopy is shown in Fig. S1). It features irregular micro/nano-structures, and together with the low surface

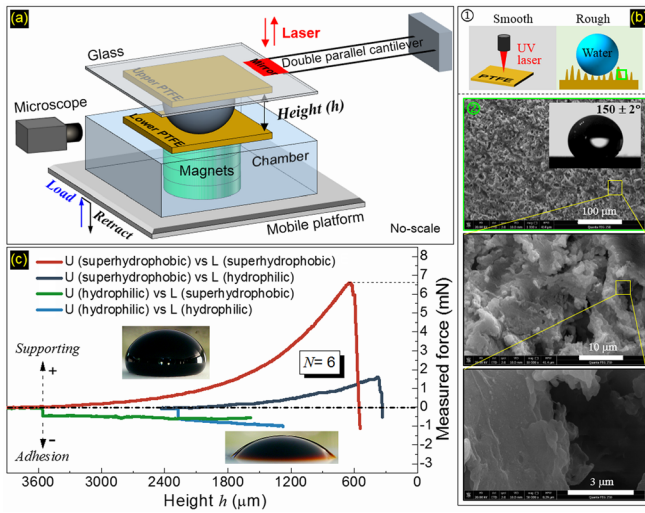


FIG. 1. (a) Schematic of the designed apparatus. (b) ① Ultraviolet laser machining and ② wetting property and progressively enlarged scanning electron microscopy images of the prepared PTFE surfaces. (c) Forces measured at PTFE interfaces of different wettability.

energy of PTFE, a liquid can remain on top of the asperities and trap air in the interstices; thus, the Cassie-Baxter state holds.¹⁹ The apparent contact angle of de-ionized water on the prepared surface is $\sim 150^\circ$.

A Fe_3O_4 water based magnetic fluid is employed, and its properties are given in Table S1. The apparent contact angle of the magnetic fluid is $\sim 142^\circ$ on the prepared surface and $\sim 45^\circ$ on a smooth one (Fig. S3). Compared to de-ionized water, the decrease in the apparent contact angle is attributed to the internal Fe_3O_4 particles and surfactant. Because the wetting property of the fabricated surfaces is close to the superhydrophobic state, they are described herein as superhydrophobic.

The experimental process is as follows. Placing a 25- μl magnetic fluid droplet on the lower PTFE surface and moving the platform upward with a speed of 10 $\mu\text{m/s}$, as the droplet comes in contact with the upper substrate, the force interaction at the interface deflects the double parallel cantilever. This deflection is measured by a laser interferometer (SP2000; SIOS Messtechnik, Germany) mounted on a fixed rack. Combined with the stiffness of the cantilever, the interfacial force can be obtained; more details about the measurement are available in our previous paper.²⁰ The entire process is recorded via a microscope, and each test is performed three times at an ambient temperature of $\sim 25^\circ\text{C}$.

Figure 1(c) shows the forces measured at the PTFE interfaces of different wettability as a function of height h for $N=6$. Positive and negative values represent supporting and adhesive forces, respectively. The differing starting point of the measured force is due to the differing initial shape of the magnetic fluid droplet. When the upper (U) substrate is hydrophilic, the adhesion effect is always present at the interfaces regardless of whether the lower (L) one is hydrophilic or hydrophobic. Supporting capacity is achieved when the upper substrate becomes superhydrophobic, and the measured supporting force of the magnetic fluid droplets at the interface of two superhydrophobic

surfaces is the highest. As indicated by the red line, it increases rapidly with decreasing h , and the maximum supporting force is ~ 6.7 mN at $h = \sim 600$ μm . Decreasing h further squeezes the droplet out of the interface, yielding a dramatic downward trend. Note that magnetic fluid droplets are unstable at the superhydrophobic interfaces without an external magnetic field; thus, the corresponding supporting force is relatively small and uncertain (Fig. S2).

The above results indicate that using an external magnetic field to limit the magnetic fluid droplets to the superhydrophobic interface can provide a supporting force. Furthermore, the dynamic response characteristics of the supporting capacity of this configuration are determined. As shown in Fig. 2, five load–retract cycles are performed on a magnetic fluid droplet at the superhydrophobic interface ($N=6$), with the inset showing one compression process. The lower substrate is retracted when the instantaneous supporting force reaches ~ 5.2 mN [smaller than the maximum force of ~ 6.7 mN shown in Fig. 1(c)]. The measured supporting forces are extremely repeatable within each load–retract cycle, having a precision as high as 98.3%. This indicates that the supporting capacity based on magnetic fluid droplets has excellent dynamic response characteristics.

Figure 3(a) shows how the magnetic field influences the supporting force, with the insets showing the initial shapes of the magnetic fluid droplets on the superhydrophobic surface for $N=1, 2, 6,$ or 10 magnets. The supporting force increases with increasing N : the force with $N=10$ is ~ 10.1 mN, which is more than twice that with $N=1$ (4.4 mN). Figure 3(b) shows the distributions of the magnetic field in a cross section above the PTFE surface. Note that the magnetic field strengthens with increasing N and becomes concentrated above the surface when $N=6$ or 10 . Figure 3(c) shows the numerical values of the magnetic field strength (Mag H) on the PTFE surface ($z=0$ mm), it being highest at the center point and decreasing gradually to the surroundings. Meanwhile, Mag H along the center decreases with increasing z , as shown in Fig. 3(d). The details of the numerical modeling are shown in Fig. S3.

Overall, the magnetic fluid-based dynamic supporting capacity is reliable and accurate, and so the supporting mechanism is analyzed further. Figure 4(a) shows the actual deformation process during compression, and one of the intermediate shapes is extracted for modeling

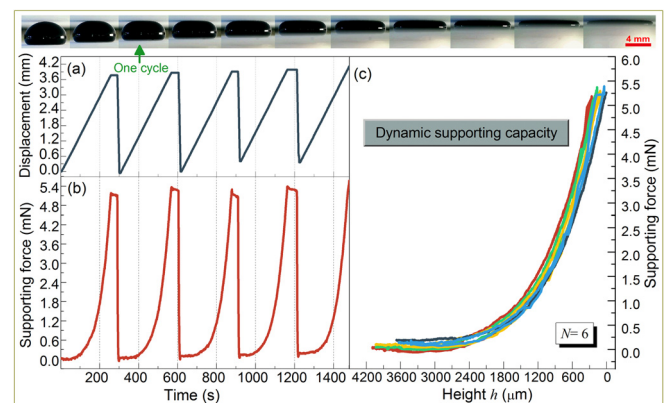


FIG. 2. Dynamic supporting capacity of a magnetic fluid droplet at a superhydrophobic interface for $N=6$: (a) details of five compression cycles; (b) loading and retracting processes; (c) dynamic supporting forces.

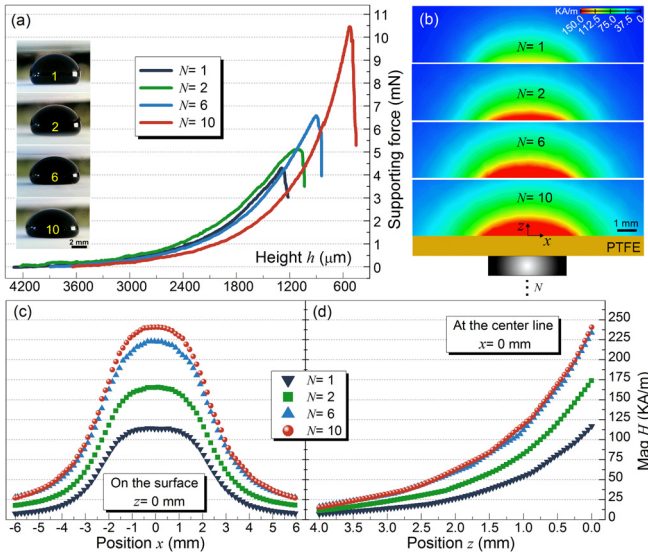


FIG. 3. (a) Influence of magnetic field on supporting force. (b) Magnetic-field distributions in cross section above PTFE surface. Numerical values of Mag H (c) on the surface ($z = 0$ mm) and (d) at centerline ($x = 0$ mm).

(labeled as 1) of which the geometrical features are defined. A curved liquid–air interface yields a Laplace pressure difference ΔP_{Lap} , and a magnetic field induces a pressure difference ΔP_{Mag} on the droplet. Following the geometry in Fig. 4(a-1), assuming that the principal radii r of curvature are equal, then r can be obtained as

$$r = \frac{\overline{AB}}{2 \cos \angle ABO} = \frac{\sqrt{h^2 + \Delta L^2}}{2 \cos \left[180^\circ - \theta_B - \arctan \left(\frac{\Delta L}{h} \right) \right]}. \quad (1)$$

The Laplace pressure difference ΔP_{Lap} is given by

$$\Delta P_{Lap} = \frac{2\gamma}{r} = \frac{4\gamma \cos \left[180^\circ - \theta_B - \arctan \left(\frac{\Delta L}{h} \right) \right]}{\sqrt{h^2 + \Delta L^2}}, \quad (2)$$

where γ is the surface tension of the liquid. Under a magnetic field, the Bernoulli equation for points i and j in the droplet at zero speed can be written as^{21,22}

$$P_i - \mu_0 \int_0^{H_i} M_s dH = P_j - \mu_0 \int_0^{H_j} M_s dH, \quad (3)$$

where μ_0 is the magnetic permeability of a vacuum and M_s is the saturation magnetization of the magnetic fluid. The magnetic pressure difference ΔP_{Mag} can be written as

$$\Delta P_{Mag} = \int_{H_i}^{H_j} P_j - P_i dH = \mu_0 M_s \int_{H_i}^{H_j} \nabla H \cdot dH = \mu_0 M_s (H_j - H_i). \quad (4)$$

Together, ΔP_{Lap} and ΔP_{Mag} contribute to a supporting force $F_{Supporting}$ directed upward, while the surface tension near the three-phase contact line of the upper substrate provides a vertical component that weakens the supporting capacity. Thus, the total supporting force can be obtained as

$$F_{supporting} = (\Delta P_{Lap} + \Delta P_{Mag}) \pi r_A^2 - 2\gamma \cos(\theta_A - 90^\circ) \pi r_A. \quad (5)$$

Combining Eqs. (2), (4), and (5), we arrive at the final expression for the supporting force, namely,

$$F_{supporting} = \left\{ \frac{4\gamma \cos \left[180^\circ - \theta_B - \arctan \left(\frac{\Delta L}{h} \right) \right]}{\sqrt{h^2 + \Delta L^2}} + \mu_0 M_s (H_j - H_i) \right\} \pi r_A^2 - 2\gamma \cos(\theta_A - 90^\circ) \pi r_A. \quad (6)$$

The apparent contact angles of magnetic fluid droplets on the prepared surfaces under varying magnetic field are measured and

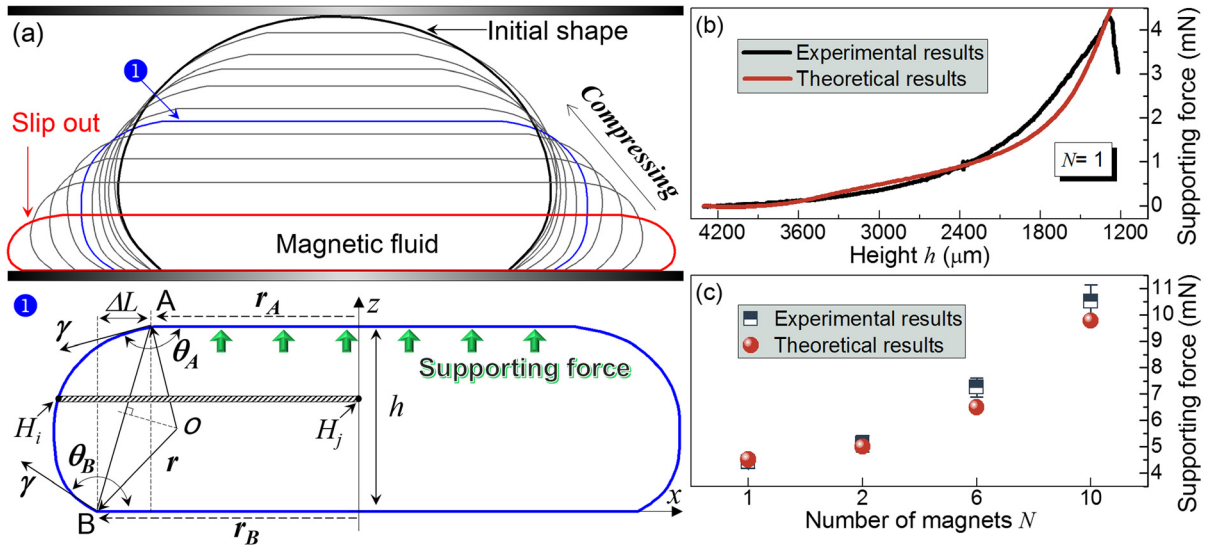


FIG. 4. (a) Actual deformation process and schematic depicting geometrical features. Comparison between experimental and theoretical results for (b) $N = 1$ and (c) varying N .

shown in Fig. S3. The theoretical supporting force is calculated by substituting all the geometrical dimensions from the recorded frames and the numerical data of the magnetic field into Eq. (6). Figure 4(b) shows the experimental and theoretical supporting forces as functions of height h for $N=1$, and Fig. 4(c) compares the theoretical and experimental results under varying magnetic field. The established theoretical model appears to be highly accurate in predicting the supporting capacity. Initially, the supporting force increases very slowly, but it increases dramatically as the droplet nears the critical state [the red line in Fig. 4(a)]. The magnetic-field distributions [Fig. 3(b)] suggest that the magnetic field is effective at limiting the magnetic fluid droplets to the interface. The robust supporting force for $N=10$ is attributed to the strong magnetic field density close to the surface, which prevents droplets from slipping out.

In conclusion, a liquid meniscus of millimeter-scale length exhibits a large Laplace pressure. By confining a magnetic fluid droplet at a superhydrophobic interface via varying external magnetic fields, the droplet remains at the small-scale liquid meniscus, thereby providing a controllable supporting force. A strong magnetic field covering the entire surface is suggested for achieving a robust and stable supporting capability. The present study provides further physical insight into liquid-based support and offers excellent prospects for a frictionless and controllable micro-platform and laboratory-on-chip applications.

See the [supplementary material](#) for the main physical parameters of the magnetic fluid, the Energy dispersive spectroscopy (EDS) result for the prepared surfaces, the forces measured at the interface of the two superhydrophobic surfaces without magnets, details of the numerical modeling, and the apparent contact angles of the magnetic fluid droplets.

The authors thank the National Natural Science Foundation of China (Grant Nos. 51875278 and 51805252) and the China Postdoctoral Science Foundation for financial support.

DATA AVAILABILITY

The data that support the findings of this study are available from the corresponding author upon reasonable request.

REFERENCES

- ¹G. Cha and Y. S. Jua, *Appl. Phys. Lett.* **94**, 211904 (2009).
- ²J. V. I. Timonen, M. Latikka, L. Leibler, R. H. A. Ras, and O. Ikkala, *Science* **341**, 253 (2013).
- ³M. H. Alheshibri, N. G. Rogers, A. D. Sommers, and K. F. Eid, *Appl. Phys. Lett.* **102**, 174103 (2013).
- ⁴M. Latikka, M. Backholm, J. V. I. Timonen, and R. H. A. Ras, *Curr. Opin. Colloid Interface Sci.* **36**, 118 (2018).
- ⁵M. Li, Q. Jiao, Q. Dai, L. Shi, W. Huang, and X. Wang, *Polym. Test.* **74**, 266 (2019).
- ⁶P. Dimitrakopoulos and J. J. L. Higdon, *J. Fluid Mech.* **435**, 327 (2001).
- ⁷B. Radoev, I. T. Ivanov, and P. Petkov, *Colloids Surf., A* **505**, 98 (2016).
- ⁸F. Dutka, Z. Rozynek, and M. Napiórkowski, *Soft Matter* **13**, 4698 (2017).
- ⁹Z. Hu, Q. Dai, W. Huang, and X. Wang, *J. Phys. D* **53**, 025002 (2020).
- ¹⁰S. G. E. Lampaert, J. W. Spronck, and R. A. J. van Ostayen, *Proc. Inst. Mech. Eng., Part J* **232**, 14 (2018).
- ¹¹J. Wen, D. Dini, and T. Reddyhoff, "Design and optimization of a liquid ring thrust bearing," *Tribol. Int.* (to be published).
- ¹²S. Sudo, D. Asano, H. Takana, and H. Nishiyama, *J. Magn. Magn. Mater.* **323**, 1314 (2011).
- ¹³I. Torres-Díaz and C. Rinaldi, *Soft Matter* **10**, 8584 (2014).
- ¹⁴C.-P. Lee, S.-T. Yang, and Z.-H. Wei, *J. Magn. Magn. Mater.* **324**, 4133 (2012).
- ¹⁵S. Afkhami, A. J. Tyler, Y. Renardy, M. Renardy, T. G. St. Pierre, R. C. Woodward, and J. S. Riffle, *J. Fluid Mech.* **663**, 358 (2010).
- ¹⁶C. Rigoni, M. Pierno, G. Mistura, D. Talbot, R. Massart, J. C. Bacri, and A. Abou-Hassan, *Langmuir* **32**, 7639 (2016).
- ¹⁷S. Manukyan and M. Schneider, *Langmuir* **32**, 5135 (2016).
- ¹⁸S. Kolhe, A. Deshpande, and K. Wangikar, *Smart Technologies for Energy, Environment and Sustainable Development* (Springer, 2019), Vol. 571.
- ¹⁹E. Y. Bormashenko, *Wetting of Real Surfaces* (De Gruyter, Berlin, 2019).
- ²⁰M. Li, W. Huang, and X. L. Wang, *Meas. Sci. Technol.* **28**, 035601 (2017).
- ²¹V. Bashtovoi, G. Bossis, P. Kuzhir, and A. Reks, *J. Magn. Magn. Mater.* **289**, 376 (2005).
- ²²Z. Wang, Z. Hu, W. Huang, and X. Wang, *J. Phys. D* **50**, 435004 (2017).